Temporal Damping Effect of the Yucca Mountain Fractured Unsaturated Rock on Transient Infiltration Pulses

Keni Zhang, Yu-Shu Wu, and Lehua Pan
Earth Sciences Division, Lawrence Berkeley National Laboratory

Abstract

Performance assessment of the Yucca Mountain unsaturated zone (UZ) as the site for an underground repository of high-level radioactive waste relies on the crucial assumption that water percolation processes in the unsaturated zone can be approximated as a steady-state condition. Justification of such an assumption is based on temporal damping effects of several geological units within the unsaturated tuff formation. In particular, the nonwelded tuff of the Painbrush Group (PTn unit) at Yucca Mountain, because of its highly porous nature, has been conceptualized to have a significant capacity for temporally damping transient percolation fluxes. The objective of this study is to investigate these damping effects, using a three-dimensional (3-D) mountain-scale model as well as several one-dimensional (1-D) models. The 3-D model incorporates a wide variety of the updated field data for the highly heterogeneous unsaturated formation at Yucca Mountain. The model is first run to steady state and calibrated using field-measured data and then transient pulse infiltrations are applied to the model top boundary. Subsequent changes in percolation fluxes at the bottom of and within the PTn unit are examined under episodic infiltration boundary conditions. The 1-D model is used to examine the long-term response of the flow system to higher infiltration pulses, while the damping effect is also investigated through modeling tracer transport in the UZ under episodic infiltration condition. Simulation results show the existence of damping effects

within the PTn unit and also indicate that the assumption of steady-state flow conditions below the PTn unit is reasonable. However, the study also finds that some fast flow paths along faults exist, causing vertical-flux quick responses at the PTn bottom to the episodic infiltration at the top boundary.

Keywords: Unsaturated Zone; Damping Effect; Yucca Mountain; Episodic Infiltration; Model.

1. Introduction

Technical considerations for selection of the Yucca Mountain site as the U.S. national high-level waste disposal site include arid climate, thick unsaturated zone, and remote location. In addition, the strategy of building the permanent subsurface repository is based on the capability of the thick UZ as a natural barrier, slowing rapid water percolation, limiting the availability of water for contacting waste and transporting radionuclides from the unsaturated zone to the saturated zone. This natural barrier idea is also supported by the presence at Yucca Mountain of several geological layers with large pore spaces, strong capillary barriers and damping effects. One of these geological layers identified during site characteriation is the layered, nonwelded PTn unit tuffs that exist between the ground surface and the repository horizon. Infiltrating water descending from the land surface may be effectively damped spatially and temporally by these layers, and thus percolation could be approximated as a steady-state condition once passing them (Montazer and Wilson, 1984; Wu et al., 2000; 2002a; 2002b).

The performance of the proposed repository for long-term storage of high-level radioactive wastes is critically dependent on the rate of UZ percolation. This is because percolation flux through the UZ is one of the most important factors in underground repository performance. The quantity as well as spatial and temporal variations in percolation flux directly affect: (a) the amount of water flowing into waste emplacement drifts; (b) moisture conditions and the corrosion environment of waste packages within the drifts; (c) waste mobilization from the potential repository; (d) thermo-hydrologic behavior of the potential repository; and (e) radionuclide migration from the UZ to the saturated zone. Net infiltration consists of only a small fraction of the total precipitation at the ground surface, representing the amount of water which penetrates the ground surface to a depth where liquid water can no longer be removed (for example, by evapotranspiration). Net infiltration is spatially varying, and its values range from several milimeters to several hundred milimeters per year, as estimated by an infiltration model using precipitation and other field data for present and future climates (Flint el al., 1996; BSC, 2004b). The infiltration data from BSC (2004b) are used for convenience only. Different infiltration distribution does not impact the results of this study.

The land-surface boundary employed by UZ models and modeling studies for the Yucca Mountain site has been traditionally described with water recharge, using estimated steady-state infiltration maps (e.g., Wu et al., 2004) i.e., temporal average infiltration rates for different time periods. However, the net infiltration is in fact episodic over seasons and years, with significant pulses probably occurring once every few years (BSC, 2004b). Spatially and temporally variable infiltration pulses act to percolate rapidly through the highly fractured tuffs of the Tiva Canyon Welded (TCw) unit, the top of the

UZ layers, as indicated by the numerous bomb-pulse chlorine-36 signatures measured within the TCw (Fabryka-Martin, 2000) and recent seepage in the south tunnel. A review of the study for fast pathways at the site has been provided by Flint et al. (2001). Down below, the character of the rock formation changes from welded tuffs to nonwelded tuffs at the TCw-PTn interface, and flow behavior changes from fracture-dominated to matrix-dominated flow (Wu et al., 2002a). Wang and Narasimhan (1985, 1993) suggested that effects of infiltration pulses at the surface are damped by the underlying tuff units, especially the PTn. The highly porous and less fractured PTn unit may attenuate the episodic infiltraton liquid flux significantly, such that the net episodic infiltration, once crossing the PTn, may be treated as steady state flow. It is believed that damping effects might be caused by lateral diversion and/or capillary barriers (Ross, 1990; Oldenburg and Pruess, 1993; Ho and Webb, 1998). The lateral diversion might reduce the volume of water that would penetrate the TSw. Flow diversion of the PTn has been confirmed by a number of modeling exercises (Ho, 1995; Wilson, 1996; Wu et al. 2002b; Pan et al., 2004).

In the past two decades, many site-specific studies have been carried out, with significant progress made in characterizing flow and transport processes at the Yucca Montain site (e.g., Wu et al., 1999; BSC, 2004a). Most of these studies, however, have been focused on analyzing the spatial variability of UZ flow and percolation patterns (for example, steady-state lateral flow resulting from capillary barriers or perched water). Very few investigations have been attempted for transient flow behavior, such as temporal damping effects (Wu et al., 2000). In the past several years, however, a limited number of

modeling efforts have investigated the temporal damping effect of the PTn unit. Those efforts primarily used one-dimensional (1-D) or two-dimensional (2-D) flow and transport models to examine the responses of vertical flux to the pulse-infitlration boundary conditions at the land surface. Wu et al. (2000) investigated how surface transient infiltration affected capillary barriers and percolation, using both one-dimensional and two-dimensional models. Their models clearly indicate the importance of PTn-unit damping effects. The model results show that the surface transient infiltration pulse can be significantly smoothened, temporally, after the early transient period of several hundreds of years. Guerin (2001) developed 1-D models to examine the flow and transport behavior in 1-D columns. These 1-D models correspond to several boreholes at the Yucca Mountain site. Guerin's models were run using different infiltration scenarios. From model calculations, she concluded that the PTn unit damped infiltration pulses no matter what infiltration scenarios were applied. Calibration results indicated that for most parameter changes, no notable movement of contaminant occurred below the PTn. Differences in contaminant transport behavior for the various simulations were only noted above the bottom of PTn unit. Other modeling studies indicate that the damping effect may be caused by lateral flow within the PTn unit (Wu et al., 2002b; Liu et al., 2003b). However, 1-D and 2-D models generally have difficulty describing the 3-D unsaturated flow system--for example, the lateral flow paths and flow focusing phenomena through heterogeneous 3-D layers of the Yucca Mountain UZ. In addition, those previous studies have not provided in-depth discussions or insights into the mechanisms of PTn damping effects.

In addition to modeling investigations, Salve et al. (2003) carried out a series of field tests for understanding flow patterns within the PTn. They examined whether the nonwelded tuffs of the PTn effectly damp pulses of infiltration, or whether preferential flow paths forming within the PTn serve to promote flow focusing. Their test results suggested that the PTn matrix has few discrete flow paths that can transmit water quickly, while the adjoining bulk matrix to the flow paths has much lower permeability. They found that episodic infiltration events appear to be damped by an initially dry PTn matrix, and that faults may convey a pulse of water over larger distances when the matrix is wet. These tests, however, are limited to a small scale in space within the PTn unit, and the test results cannot show large-scale effects of the flow system. Faybishenko et al. (2003) made an effort to understand the testing results through analysis of the temporal variations of the infiltration rates, using three different scale infiltrations: macro-scale, meso-scale, and micro-scale.

The objective of this study is to provide an in-depth modeling analysis of the effectiveness of the PTn unit in damping effects of using both 3-D mountain-scale model and 1-D vertical columns model. The focus of this work is on the transient, temporal aspect of flow smoothing and damping by the PTn unit. The 3-D model is used to examine PTn damping effects in both space and time. The 1-D vertical flow model is used to investigate long-term responses of the vertical flow system to high infiltration pulses, under different rates and durations of infiltration pulses. Moreover, a 1-D tracer transport model is also run to further analyze the damping effect at the PTn unit. The 3-D model is based on what has been developed for currently investigating unsaturated zone

flow and transport process at the Yucca Mountain site (Wu et al., 2004). The model incorporates a wide variety of field data and the current geological framework model to describe the highly heterogeneous formation at Yucca Mountain. In this study, the 3-D model is first run to steady state under present-day mean infiltration and calibrated using field-measured data. Then, pulse infiltrations are applied to the top boundary. The temporal average of the infiltration pulses is assumed to be equivalent to the value of the steady-state mean infiltration at present-day climates. The damping effect is investigated by examining percolation flux and moisture changes in the UZ under episodic infiltration boundary conditions against steady-state infiltration. Damping effects may be caused by different geological conditions and mechanisms. Mechanisms of damping effects are revealed through calculation of percolation flux and its spatial and temporal allocation. Model results indicate the existence of significant damping effect of the PTn unit. However, fast flow paths may develop along faults, which may cause a quick vertical-flux response at the PTn bottom to the episodic infiltration at the land surface.

2. Model Development

The 3-D model used in this study is based on the site-scale UZ flow model (Wu et al., 2004; BSC, 2004a). The difference is that transient infiltration conditions are described in the current study for different pulsed-infiltration scenarios. The model is described as follows.

2.1 Hydrogeological and Conceptual Model

The Yucca Mountain UZ comprises alternating layers of welded and nonwelded tuffs (Figure 1). The major formations have been organized into several hydrogeological units, based roughly on the degree of welding within each unit (Montazer and Wilson, 1984). At the top is the welded Tiva Canyon Tuff (TCw), followed sequentially by the Yucca Mountain, Pah Canyon, and the Topopah Spring Tuffs of the Paintbrush Group (PTn). The nonwelded tuffs of the PTn unit lie immediately above the welded tuff of the Topopah Spring Tuff (TSw), the host rock for the proposed nuclear waste repository. Below the TSw unit is the Calico Hills nonwelded (CHn) unit and the Crater Flat undifferentiated (CFu) unit. Figure 1 shows a typical vertical cross section of the UZ formation in the east-west direction. The aerial domain of the model encompasses approximately 40 km^2 (Figure 2).

The PTn unit, on which this study will focus, primarily consists of non- to partially welded tuffs and extends from the base of the densely-to-moderately welded, crystal-poor vitric subzones of the Tiva Canyon Tuffs to the top of the densely welded, crystal-rich vitric subzone of the Topopah Spring Tuff. Table 1 shows the relationshhip between hydrogeologic units, geological units, and associated model layers for the TCw and PTn unit. Sublayers in the PTn unit are each less than 10 m thick within the potential repository footprint, and several layers show considerable variation in thickness across the potential repository area (with each showing a thinning trend to the south). The combined thickness of the PTn layers exceeds 150 m at the northern end of Yucca Mountain, while at the southern end, the PTn thins to less than 30 m or even pinched out.

Within the proposed repository area (Figure 2), the thickness of the PTn unit ranges from approximately 30 to 60 m. The dip of PTn sublayers is generally to the east at about ten degrees or less.

Besides the highly heterogeneous nature of the fractured, layered tuffs, the unsaturated flow in the area is further complicated by numerous strike-slip and normal faults with varying amounts of offset (Scott and Bonk, 1984). The vertical offset along these faults commonly ranges from ten to hundreds of meters and generally increases from north to south. These major faults are generally vertical or near-vertical and penetrate the entire UZ thickness, and to a certain extent they control moisture flow and saturation distributions. The major faults included in the model are shown on Figure 2, because they are important features and may provide fast pathways for flow and transport or serve as barriers to lateral flow (Wu et al., 2000).

Three key assumptions for the conceptual model used in this study are: (1) the hydrogeological units/layers are internally homogeneous, and the material properties of each unit (defined by previously calibrated parameters; Liu et al., 2003) are continuous throughout each layer, unless interrupted by faults; (2) water flow in the system is at a steady-state condition before the episodic infiltration condition applied on the surface boundary; and (3) faults are represented by vertical or inclined columns of gridblocks having finite width. More detailed description of the 3-D mountain-scale model can be found at BSC (2004a).

2.2 Boundary Conditions

The 3-D model domain includes boundaries at the top, bottom, and four sides (Figures 1 and 2). Mountain ground surface is treated as the top model boundary, and the water table is treated as the bottom boundary. In simulation, pulse infiltration is applied on the top boundary as a source term to fractures. The bottom boundary, the water table, is treated as a Dirichlet-type boundary. All the lateral boundaries are treated as no-flow boundaries. The top pulse-infiltration boundary condition is set by concentrating a total amount of net infiltration, averaged over 50 years, to the modeling domain in one week as infiltration pulses. Temporal average for infiltration pulses is assumed to be the present-day mean infiltration rate. The model's top boundary is subject to nonzero infiltration (with a pulse of 2,609 times present-day mean infiltration) for only one week every 50 years, while during the rest period of every 50 years, the surface boundary is subject to zero infiltration. This assumption provides an extreme condition, which is conservative for the investigation of the PTn damping effect. Moreover, for examining the influence of infiltration rate and pulse length on the UZ flow system, higher infiltration rates and longer pulse lengths are also applied to the model.

Net infiltration of water resulting from precipitation that penetrates the topsoil layer of the mountain is considered the most important factor affecting the overall hydrological, geochemical, and thermal-hydrologic behavior of the UZ. This is because net infiltration is the ultimate source of groundwater recharge and percolation through the UZ. A steady-state net infiltration map used in this study is generated based on the estimates by the BSC (2004b) for the site. The spatial distribution of the infiltration pulse rates, as

interpolated onto the model grid, is shown in Figure 3. This figure shows that higher recharge rates are located in the northern part of the model domain and along the mountain ridge from south to north.

2.3 Numerical Modeling Approach

In evaluating fluid flow in the unsaturated fractured tuffs, we treated fracture and matrix flow using a dual-permeability modeling approach. The model domain was discretized into irregular model grids, with relatively refined grid meshes within the repository footprint and along the several faults. The model grid consists of 2,042 columns (or gridblocks per grid layer) of both fracture and matrix continua, and averages 59 computational grid layers in the vertical direction, resulting in approximately 250,000 gridblocks and 1,000,000 connections. The plan view of the 3-D model domain, grid, and incorporated major faults is presented in Figure 2.

In this modeling study, the variably saturated flow is considered as single aqueous phase. The gas pressure and temperature are assumed to be constant. Liquid flow is described by a generalized form of Richards' equation:

$$\frac{\partial}{\partial t}(\phi S \rho) = div\,[k \frac{k_r}{\mu} \rho \nabla (P + \rho g z)] \qquad (1)$$

where ϕ is medium porosity, S is water saturation, ρ is water density, μ is viscosity, k is absolute permeability, k_r is relative permeability for water, g is gravitational acceleration, and P is pressure. The van Genuchten model of relative permeability and capillary

pressure function (van Genuchten, 1980) is adopted to describe the relationships between relative permeability, capillary pressure, and saturation.

This large-scale transient flow problem was expected to involve extensive computational efforts. Numerical simulations of modeling studies were carried out using the parallel version TOUGH2 code (Zhang et al., 2001), which uses the same numerical schemes as the original TOUGH2 (Pruess, 1991). The parallel code was used to solve Equation (1) for unsaturated flow on the IBM SP super computer using 64 or 128 processors.

3. Results and Analysis

The PTn unit's temporal damping effect on percolation fluxes is examined through 3-D and 1-D flow and transport models, with episodic infiltration pulses applied to the top model boundary. In general, spatially and temporally variable pulses of flow percolate rapidly through the highly fractured tuffs of the TCw. At the TCw-PTn interface, where welded tuffs change sharply into nonwelded tuffs, flow behavior changes from fracture-dominated to matrix-dominated flow (Wu et al., 2002a). The highly porous and less fractured PTn unit has a large potential for attenuating the episodic infiltration flux either by imbibition of water into the rock matrix and/or diverting water to faults.

3.1 3-D Model Results

Table 2 presents the 3-D model's simulated total vertical flux at the interface between the PTn and TSw unit at different times. The results for the first 100 years following infiltration pluses applied are included in the table. Before application of infiltration pulses on the model top boundary, the UZ flow system is in a steady state. The steady-

state condition was reached by running the model with present-day mean infiltration applied on the top boundary. Because of the computing-time involved in large-scale transient flow simulations, only 100-year 3-D simulations were run. For a 100-year simulation, more than 50 hours of computing time are needed on a supercomputer using 128 processors. Table 2 shows that simulated percolation fluxe at the PTn bottom vary with time under episodic infiltration, but the magnitude of the transient variation of the total fluxes is relatively small compared to the infiltration pulse on the land surface, which has a rate of 14,584 kg/s. The total flux shows a quick response to each infiltration pulse. However, most quick response fluxes move through faults to reach the PTn bottom. If fluxes through faults are excluded, the fluctuation of total percolation flux at the PTn bottom is small, less than 1% of the total flux change. Simulation results indicate that after the infiltration pulse, the total fluxes at the PTn bottom gradually approach the average value of the present-day mean infiltration rate (5.59 kg/s), and eventually the system will reach the equilibrium of present-day mean infiltration boundary conditions.

Figure 4 demonstrates the vertical flux change at the PTn bottom between the beginning (100 years) and end (100 years+1 week) of the third infiltration pulse. The locations with the most signficant flux changes are at or near faults. Flux changes range from 0 to several 10s of millimeters per year. The figure clearly indicates that faults serve as quick flow channels. Most water reaches the PTn bottom through faults (such as the Sever Wash fault, Ghost Dance fault, the north part of Solitario Canyon fault, and Drillhole Wash fault). Other faults (or part of a fault) may not respond so quickly to the infiltration pulse at the land surface--for example, the Pagany Wash fault, the south part of the Drillhole Wash fault, and the Solitario Canyon fault. This could be caused by lower net

infiltration distributed above these faults. Faults under thick alluvium, which reduces the amount of net infiltration, will not develop as fast pathways through the PTn. A detailed discussion of the mechanism and a conceptual model of the development of fast paths through the PTn can be found at Flint et al. (2001). In the areas without faults, fast vertical-flux response to the top infiltration pulses does not occur.

To investigate flux changes inside the unsaturated zone under episodic infiltraton condition, we examined flux variations through typical vertical columns. Figure 5 shows the vertical fluxes at column "o50" right before and after an infiltration pulse was applied at the top boundary. Column o50 is located at Nevada coordinate 170,790m, 230,720m (see Figure 2), which is at the south of the model domain and has a thinner PTn layer compared to the north part of the domain. The thinner PTn layer may demonstrate relatively weaker damping effect. Figure 5 indicates that flux can move rapidly through the TCw unit and enter the top sublayers of PTn. Vertical flux at the TCw/PTn interface has an almost instant response to the top infiltration. This result is consistent with field testing results conducted at the site and the small-scale model analysis for the tests (Liu et al., 2003a). The influence zone of infiltration pulse from land surface ends inside the PTn layer. This is demonstrated by the simulated vertical flux, after passing several top sublayers of the PTn unit, becomes identical for both before and after infiltration pulse is applied. Figure 6 shows vertical fluxes at column "f96" (at Nevada coordinate 170,890 m, 235,050 m; see Figure 2) at different times. The column f96 was selected because it is located near the center of the repository footprint and is a typical column for the repository area. Right after an infiltration pulse is applied at the top boundary (100 years+1week), vertical flux reaches its maximum. After ceasing pulse infiltration, the

vertical flux in TCw and the top PTn subunits gradually attenuates, approaching the flux at the beginning of the infiltration pulse (100 years). Figure 6 indicates that the percolation flux shows little change at the elevation of 1,315 m or below (at the bottom of the PTn4 subunit). These results confirm that a damping effect occurs at the PTn unit, especially in the PTn1-PTn4 subunits.

The damping effect could be caused by several geological features at the site. Lateral flow diversion by capilliary barriers and imbibition into rock matrix may be the two most important factors. Capillary barriers form in unsaturated zones where a layer containing relatively fine pores or fractures overlies a layer containing relatively coarse pores or fractures. Such capillary barriers within the PTn unit could promote lateral flow and retard the rate of percolation. Discussion of capilliary barriers within the PTn unit can be found at Wu et al. (2000, 2002b) , Pan et al. (2004), and Flint et al. (2003). The stratified features may assist in preventing water from entering the underlying TSw units during episodic infiltration events. The period of no infiltration after episodic infiltration allows the PTn rock matrix to desaturate before it is recharged by the next infiltration event. Thus, the additional pore space in the dryer PTn matrix provides a storage capability that prevents a rapid through-flow of water percolation.

Field tests by Salve et al. (2003) demonstrate that early episodic infiltration events can be effectively damped by the initially dry PTn matrix, even if the flow is through a fault path. By examining matrix saturation and capilliary pressure at the model columns, we can find only a small portion of the columns demonstrating minor changes after applied pulse infiltration. Figure 7 shows simulated matrix saturation right before and after an infiltration pulse applied at the top boundary for the column of borehole SD-12 (model

column q47), and field-measured saturation data at the location. In general, the modeled results for the two times are in reasonable agreement with the measured saturation data. The figure indicates that the infiltration pulse causes matrix-liquid saturation changes only at the TCw bottom and PTn top sublayers, within a range of about 15 m. For the one-week period when infiltration pulses are applied, the increased amount of water storage in matrix blocks at the column is 1.03×10^6 kg, and the total amount of infiltration at the top of this column is 0.8×10^6 kg. The storage increase is larger than the total infiltration water at the column. This result may indicate that most of the pulse-infiltrating water is imbibed into the rock matrix and moves laterally. By comparing the pulse infiltration rate (14,589.32 kg/s) with the total flux at PTn bottom (188.2 kg/s, peak flux), we can conclude that at least 98.7% pulse infiltration water is buffered by imbibition to matrix blocks and resaturating fractures, and less than 1.3% of the water reaches the PTn bottom through fast flow paths (faults). This finding indicates that the pulse infiltration at the top boundary has very limited influence on flow behavior below the PTn unit. Thus, the large pore storage capacity within the PTn matrix serves as a cushion, preventing a rapid through-flow of water percolation. Field tests by Salve et al (2003) have confirmed these phenomena.

Note that the pulse infiltration can only cause a minor matrix saturation change. Simulated liquid saturation profiles from the episodic boundary condition at 100 years+1week were compared against steady-state simulation results and observed profiles at borehole SD-9 and UZ-14 (Figure 8a and 8b). The simulated saturation profiles were extracted from the 3-D models, whereas the borehole data came from field measurements. As shown in the two figures, the simulated saturation profiles (for

episodic boundary conditions and steady-state solutions) are almost identical, and both are generally in good agreement with measured saturation profiles at the two locations. These results indicate that substantial matrix pore space is still available for damping water, and that the UZ can damp even higher and longer infiltration pulses.

Damping mechanisms can be further analyzed by looking into the flux allocation inside the UZ vertical columns. Infiltrating water, once it percolates into the top-soil layer through fractures, can be imbibed into dryer rock matrix, diverted to faults or other flow paths, detained along fractures, or continue percolating downward. Table 3 lists percolation flux allocations right before the beginning (100 years) and end (100 years+1week) of the third infiltration pulse at three columns: q47 (Borehole SD-12), B16, and C25. Columns B12 and C25 (see Figure 2 for their locations) are typical fault columns, demonstrating rapid responses to transient flow at the bottom to top infiltration pulses (see Fgure 4). Before the infiltration pulse is applied at the top model boundary at 100 years, the percolation flux leaving the bottom boundary of column q47 comes from fracture and matrix storage. The stored water contributes 91.7% to bottom flow and 8.3% to lateral flow leaving the column. At the end of the infiltration pulse (100y+1week), two sources of water enter to the column, infiltration (52.9%) and lateral flow (47.1%), and 99.95% of this combined water is absorbed by dry fractures and imbibed into rock matrix. These statistics are consistent with the above matrix-saturation-analysis results, which indicate that the amount of water storage increase in column q47 during an infiltration pulse is larger than the total infiltrating water applied at the column's top boundary.

Within fault columns, flux allocation is significantly different. Table 3 shows that lateral flow is the most important source contributing to the bottom flux before the infiltration pulse is applied (at 100 years)--86.5% for column B16 (the rest comes from the release of rock storage) and 100% for column C25. In column C25, about 53% water from lateral flow still remains in the column. At 100years+1week, infiltrating water from the top boundary is distributed in three ways: lateral flow (3.1% for B16, 30.6% for C25), storage increase (96.6% for B16, 69% for C25), and flux at bottom boundary (0.3% for B16, 0.4% for C25). The above flux-allocation-analysis results suggest that the damping effect at nonfault columns is mainly caused by rock storage change through absorbing and releasing water at different periods. Along fault columns, both lateral flow and matrix rock storage play an important role. The importance of these two components may be location dependent.

From the above discussion, we can conclude that the damping effect does exist in several hydrogeological units. Theoretically speaking, however, if an infiltration pulse is large and lasts long enough, the PTn damping effect may decline, and the flux below the PTn unit would eventually respond to these infiltration pulses. This can be analyzed by using different lengths of infiltration pulse to investigate responses of the flow system. Infiltration pulses (with the same rate) for 1 week, 2 weeks, 1 month, and 2 months were applied on the model top boundary at time 100 years. Figure 9 shows vertical fluxes in column q54 (for its location, see Figure 2) right before an infiltation pulse is applied (100 years) and the ends of different length infiltration pulses. It is clear that percolation fluxes can quickly run through TCw without any delays. After percolating through the TCw/PTn interface, the flux intersects the top sublayers of the PTn unit and is damped

dramatically. The longer the infiltration pulse, the further the flux fronts are pushed down into the PTn unit. However, even the longest pulse under analysis cannot break through the top several PTn sublayers. Flux distribution for 100 years (at the beginning of the infiltration pulse) demonstrates that even for a period of 50 years without infiltration from model top boundary, the flux in PTn lower sublayers does not show attenuation. The longer infiltration pulse may represent a higher average rate for an episodic infiltration period and provide an even more conservative estimation for future climate conditions.

The vertical percolation fluxes at the TCw and PTn interface change significantly with infiltration pulses. At the end of each infiltration pulse, the total flux rate at the interface is approximately equal to the pulse infiltration rate at the surface. At the beginning of an infiltration pulse, the total flux at the surface is near 0. This indicates the quick response of flux at the TCw/PTn interface to changes in surface infiltration and confirms that the damping effect happens mainly inside the PTn unit.

3.2 1-D Model Results

To investigate the long-term temporal response of the unsaturated flow system to episodic surface infiltration, we developed a one-dimensional model for a typical column from the site. The 1-D model consists of a single vertical column, extracted directly from the three-dimensional model (column b26 of the 3-D model). The column is located at Nevada coordinates 171,250.5 m, 236,250.0 m. Two different infiltration pulses, 5 mm/yr and 20 mm/yr, are used in the 1-D model study. Surface infiltration pulses are also assumed to be uniformly distributed spatially, with a one-week infiltration cycle of 50

years, i.e., the model top boundary is subject to non-zero infiltration for only one week every 50 years. The net infiltration value of the week, averaged over 50 years, is 5 mm/yr or 20 mm/yr.

Moreover, we developed a tracer transport model with constant and episodic infiltration boundary conditions, using the T2R3D code (Wu et al, 1996). The conceptual model, flow boundary conditions, simulation grids, and the basic hydrological properties of the 1-D transport model are the same as those used in the 1-D flow model. An initial constant concentration source is applied to the fracture block at the top model boundary. This boundary condition implies that a tracer is instantaneously released at the starting time of a simulation. The dispersivities for both fracture and matrix continua in the simulation are assumed to be zero. A constant molecular diffusion coefficient of 2.032E-9 m^2/s is used for matrix diffusion, and the sorption coefficient is set to zero.

Flow simulation results

Figures 10 and 11 plot variations of total fluxes versus times at the bottom of the PTn for the 5 mm/year and 20 mm/year infiltration pulses, respectively, showing slow responses in flux change at the PTn bottom. Figure 10 and 11 show flux fluctuation during the first several hundred years. The total fluxes at the bottom boundary of the PTn gradually approach their average values, and eventually the system reaches a dynamic equilibrium condition under the uniform pulses of infiltration for time greater than 1,000 years. These results clearly indicate the significance of PTn temporal damping effects and that surface infiltration or pulses can be effectively smoothed temporally after the early transient period of several hundred years. Figure 11 may imply that the damping effect will not weaken for the pulses with higher average infiltration rate. The average infiltration rate

of 20 mm/yr represents possible future climate conditions for the Yucca Mountain site. In addition, we have also examined the 1-D model results with infiltration pulses of annual average infiltration rates from 40 to 200 mm/yr. For the different infiltration pulses, the total fluxes at the PTn bottom do not demonstrate significant shifting from average infiltration rates. These results further confirm that the damping effect will not weaken for certain ranges of infiltration pulses. The 1-D model results also confirm the conclusion from the 3-D model, that most of the infiltrating water is damped by matrix imbibition, because no faults are included in the 1-D model.

Unlike the 3-D model, the 1-D model neglects the influence of lateral flow. Flow percolates in the vertical direction only. The damping effect can only be caused by storages of flux in fracture and rock matrix pores. From the change of fracture and matrix saturation, we can estimate the increase in the water storage in the column after an infiltration pulse applied. Infiltration pulses cause water storage changes mainly in the TCw and upper two subunits of the PTn. Table 4 shows the mass changes at gridblocks representing the TCw and upper part of PTn for the case of a 20 mm/year infiltration pulse applied at 1,950 years. Results shown in the table indicate that about 99.5% of total infiltration water is stored in TCw and the two top PTn sublayers, including 86.6% by imbibition to rock matrix and 12.9% by saturating fractures. The episodic infiltration water first saturates the desaturated fractures, and then imbibes into the rock matrix. Most infiltration water is buffered by the rock matrix of PTn1 and PTn2 subunits.

Transport simulation results

Transport simulation results show the influence of episodic infiltration on tracer transport, further supporting the conclusion of the existence of damping effect in the PTn. Figure 12 shows the concentration distribution in both fracture and matrix continuum at times of 200 years and 1,000 years. The concentration peak reaches the PTn top border in less than 200 years. The peak is located at PTn1 at 200 years, and then moves down about 16 m in 800 years afterward to PTn3. The concentration pulse attenuates and widens as it moves down. The two cases with constant infiltration (5 mm/year) and episodic infiltration boundary conditions produce very similar concentration-distribution patterns, except that the model with episodic infiltration predicts higher concentration retention in the matrix continuum right above the TCw/PTn interface. Figure 12 indicates that the infiltration pattern has little influence on concentration distributions below the PTn unit. The transport model results thus further show that damping effects exist in the PTn unit.

4. Summary and Concluding Remarks

We present a systematic modeling study of damping effects in the unsaturated zone at Yucca Mountain, using both 3-D mountain-scale and 1-D vertical column models. The 3-D model incorporates a wide variety of field-specific data for the highly heterogeneous formation at the site and provides a more realistic representation, while the simplified 1-D flow and transport models are useful for examining the long-term response of the flow system to different infiltration pulses.

The modeling studies indicate that the PTn unit can attenuate the episodic infiltration flux significantly. Episodic infiltration, once crossing the PTn unit, can be approximated as steady state. This study provides insights into unsaturated zone flow behavior under episodic infiltration conditions, as well as the role of the PTn unit in damping of pulse percolation. Model results show that the total percolation fluxes at the PTn bottom gradually approach the average value of mean infiltration rate for the whole period, and that eventually the system should reach a dynamic equilibrium condition under the uniform pulses of infiltration. In the areas without faults, vertical flux at the PTn bottom does not rapidly respond to top boundary infiltration pulses. Modeling results indicate that the damping effect happens at the PTn1-PTn4 subunits. Results from the 1-D model with higher-rate infiltration scenarios confirm that the damping effect will not be weakened by higher rate infiltration pulses. The transport model results further reveal that the damping effect exists specifically in the PTn unit. This study justifies the reasonableness of assuming steady-state flow conditions below the PTn unit.

Modeling results show that most percolating water is damped by the subunits at the top of PTn, and that a small percentage of percolation flux is diverted into faults. The highly porous PTn unit attenuates episodic infiltration flux by imbibing water into the rock matrix. Flux allocation analyses suggest that the damping effect at nonfault columns is mainly caused by matrix rock water storage, absorbing and releasing water at different periods. Along fault columns, both lateral flow and rock water storage play an important role with the importance of these two damping components being location-dependent.

5. Acknowledgments

The authors would like to thank Yongkoo Seol ,Dan Hawkes and anonymous reviewers for their review of this paper. We would also like to thank Diana Swantek for her help in preparing the figures. This work was in part supported by the Director, Office of Civilian Radioactive Waste Management, U.S. Department of Energy, through Memorandum Purchase Order EA9013MC5X between Bechtel SAIC Company, LLC and the Ernest Orlando Lawrence Berkeley National Laboratory (Berkeley Lab). The support is provided to Berkeley Lab through the U.S. Department of Energy Contract No. DE-AC03-76SF00098.

6. References

BSC (Bechtel SAIC Company) 2004a. UZ Flow Models and Submodels, MDL-NBS-HS-000006, REV02, Las Vegas, Nevada: Bechtel SAIC Company. ACC: DOC. 20041101.0004; DOC. 20050629.0003.

BSC (Bechtel SAIC Company) 2004b. Simulation of Net Infiltration for present-Day and Potential Future Climates. MDL-NBS-HS-000023 REV 00, Las Vegas, Nevada: Bechtel SAIC Company. ACC: DOC, 20041109.0004.

Flint, A.L., Flint, L.E., Bodvarsson, G.S., Kwicklis E., and Fabryka-Martin, J.T., 2001. Evolution of the conceptual model of unsaturated zone hydrology at Yucca Mountain, Nevada. J. of Hydrology, 247, 1-30.

Flint, A.L., Hevesi, J.A., Flint, L.E., 1996. Conceptual and numerical model of infiltration for the Yucca Mountain area, Milestone 3GU1623M, Water Resour. Invest. Rep. U.S. Geological Survey, Denver CO.

Flint, L.E., Flint, A.L., and Selker, J.S, 2003. Influence of transitional volcanic strata on lateral diversion at Yucca Mountain, Nevada. Water Resour. Res., 39(4), 1-17.

Guerin, M., 2001. Tritium and ^{36}Cl as constraints on fast fracture flow and percolation flux in the unsaturated zone at Yucca Mountain. J. of Cont. Hydrol., 51, 257-288.

Ho, C.K., 1995. Assessing alternative conceptual models of fracture flow, In: Proceedings of the TOUGH Workshop '95, Lawrence Berkeley National Laboratory, Report, LBL-37200, Berkeley, CA.

Ho, C.K. and Webb S.W., 1998. Capillary barrier performance in heterogeneous porous media. Water Resour. Res., 34(4), 603-609.

Faybishenko, B., Bodvarsson, G.S., Salve, R., 2003. On the physics of unstable infiltration, seepage, and gravity drainage in partially saturated tuffs. J. of Cont. Hydrol., 62-63, 63-87.

Fabryka-Martin, J.T., 2000. Analysis of geochemical data for the unsaturated zone, Report ANL-NBS-GS-00004, Los Alamos National Laboratory, CRWMS M&O.

Liu, H.H., Ahlers, C.F., Mukhpadhayay, S., and Wu, Y.S., 2003. Calibrated properties model, Report: MDL-NBS-HS-000003 REV 01, Lawrence Berkeley National laboratory, Las Vegas, Nevada, Bechtel SAIC Company.

Liu, H.H.; Haukwa, C.B.; Ahlers, C.F.; Bodvarsson, G.S.; Flint, A.L.; and Guertal, W.B. 2003a. Modeling flow and transport in unsaturated fractured rock: an evaluation of the continuum approach. J. of Cont. Hydrol., 62-63, 173-188.

Liu, J., Sonnenthal, E.L., Bodvarsson, G.S., 2003b. Calibration of Yucca Mountain unsaturated zone flow and transport model using porewater chloride data. J. of Cont. Hydrol., 62-63, 213-235.

Montazer, P., and Wilson, W.E., 1984. Conceptual hydrological model of flow in the unsaturated zone, Yucca Mountain, USGS Water Resources Investigation Report 84-4345.

Oldenburg, C.M., and Pruess K., 1993. On numerical modeling of capillary barriers. Water Resour. Res., 29(4), 1045-1056.

Pan, L., Wu, Y.S., and Zhang, K., 2004. A modeling study of flow diversion and focusing in unsaturated fractured rocks. Vadose Zone Journal, 3:233-246.

Pruess, K., 1991. TOUGH2 – A general-purpose numerical simulator for multiphase fluid and heart flow. Report LBNL-29400, Lawrence Berkeley National Laboratory, Berkeley, California.

Ross, B., 1990. The diversion capacity of capillary barriers. Water Resour. Res., 26(10), 2625-2629.

Salve, R., Oldenburg, C.M., Wang, J.S., 2003. Fault-matrix interactions in nonwelded tuff of the Paintbrush Group at Yucca Mountain. J. of Cont. Hydrol., 62-63, 269-286.

Scott, R.B. and Bonk, J., 1984. Preliminary geologic map of Yucca Mountain, Nye County, Nevada, with geologic sections, U.S. Geological Survey Open-File Report 84-494.

van Genuchten, M.T., 1980. A closed-form equation for predicting the hydraulic conductivity of unsaturated soils. Soil Sci. Soc. Amer. J, 44(5): 892-898.

Wang, J.S.Y. and Narasimhan, T.N., 1985. Hydrologic mechanisms governing fluid flow in a partially saturated, fractured, porous medium. Water Resour. Res., *21*(12), 1861-1874.

Wang, J.S.Y. and Narasimhan, T.N., 1993. Unsaturated flow in fractured porous media." Chapter 7 of *Flow and Contaminant Transport in Fractured Rock.* Bear, J.; Tsang, C-F.; and de Marsily, G., eds. San Diego, California: Academic Press.

Wilson, M.L., 1996. Lateral diversion in the PTn unit: capillary-barrier analysis. In: Proceedings of the High Level Radioactive Waste Management Seventh Annual International Conference. Las Vegas, NV, April 29-May 3, La Grange Park, III., American Nuclear Society, SAND95-2186C, pp.111-113.

Wu, Y.S., Ahlers, C.F., Fraser, P., Simmons, A., and Pruess, K., 1996. Software qualification of selected TOUGH2 modules, Report: LBNL-39490, Lawrence Berkeley National laboratory.

Wu, Y.S.; Haukwa, C.; and Bodvarsson, G. S., 1999. A site-scale model for fluid and heat flow in the unsaturated zone of Yucca Mountain, Nevada. J. of Cont. Hydrol., 38 (1-3), pp.185-217.

Wu, Y-S., Zhang, W., Pan, L., Hinds, J., and Bodvarsson, G.S., 2000. Capillary barriers in unsaturated fractured rocks of Yucca Mountain, Nevada, LBNL-46876, Lawrence Berkeley National Laboratory.

Wu, Y.S., Pan, L., Zhang, W., and Bodvarsson, G.S., 2002a. Characterization of flow and transport processes within the unsaturated zone of Yucca Mountain, Nevada. J. of Cont. Hydrol., 54, 215-247.

Wu, Y.S., Zhang, W., Pan, L., Hinds, J., and Bodvarsson, G.S., 2002b. Modeling capillary barriers in unsaturated fractured rock. Water Resour. Res., *38*, (11), 35-1 through 35-12.

Wu, Y.S., Lu, G., Zhang, K., Bodvarsson, G.S., 2004. A mountain-scale model for characterizing unsaturated flow and transport in fractured tuffs of Yucca Mountain. Vadose Zone Journal, 3:796-805.

Zhang, K., Wu, Y.S., Ding, C., Pruess, K., and Elmroth, E., 2001. Parallel computing techniques for large-scale reservoir simulation of multicomponent and multiphase fluid flow. Paper SPE 66343, Proceedings of the 2001 SPE Reservoir Simulation Symposium, Houston, Texas.

Figure 1. Schematic showing hydrogeological profiles and layers with possible damping effects along a typical cross section of the Yucca Mountain in the east-west direction

Figure 2. Plan view of the three-dimensional model grid, showing the model domain, faults incorporated, proposed repository footprint, and locations of columns to be investigated

Figure 3. Spatial distribution of pulse infiltration applied over the 3-D model domain, equivalent to the case of present day mean infiltration

Figure 4. Change in percolation flux at the PTn bottom after 100 years when an infiltration pulse is applied on top boundary

Figure 5. Percolation flux distribution along column o50, right before and after an infiltration pulse is applied at 100 years

Figure 6. Flux distribution along column f96 at different times: right before infiltration pulse applied (100 years), and right after an infiltration pulse applied (100 years+1 week), and afterwards

Figure 7. Matrix saturation distribution along column q47 (borehole SD-12) right before and after infiltration pulse applied at 100 years

Figure 8. Comparison of simulated liquid saturations for episodic boundary condition and steady-state infiltration results with observed matrix liquid saturation for boreholes SD-9 and UZ-14, (a) SD-12; (b) UZ-14.

Figure 9. Flux distribution along column q54 for different lengths of infiltration pulses with the same average infiltration value at 100 years

Figure 10. Simulated variations in total percolation fluxes versus times at the bottom of the PTn unit of the 1-D model, subject to one-week transient infiltration pulses every 50 years, equivalent to 5 mm/yr averaged infiltration rate

Figure 11. Simulated variations in total percolation fluxes versus times at the bottom of the PTn unit of the 1-D model, subject to one-week transient infiltration pulses every 50 years, equivalent to 20 mm/yr averaged infiltration rate

Figure 12. Simulated tracer concentration profiles; (a) in fracture, 200 years; (b) in matrix, 200 years; (c) in fracture, 1,000 years; and (d) in matrix, 1,000 years

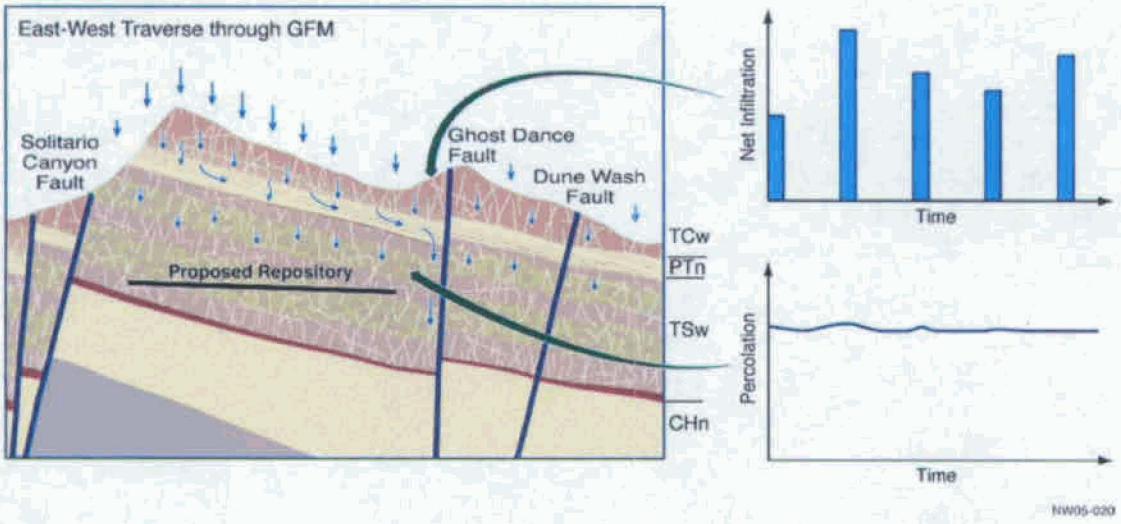

Figure 1. Schematic showing hydrogeological profiles and layers with possible damping effects along a typical cross section of the Yucca Mountain in the east-west direction

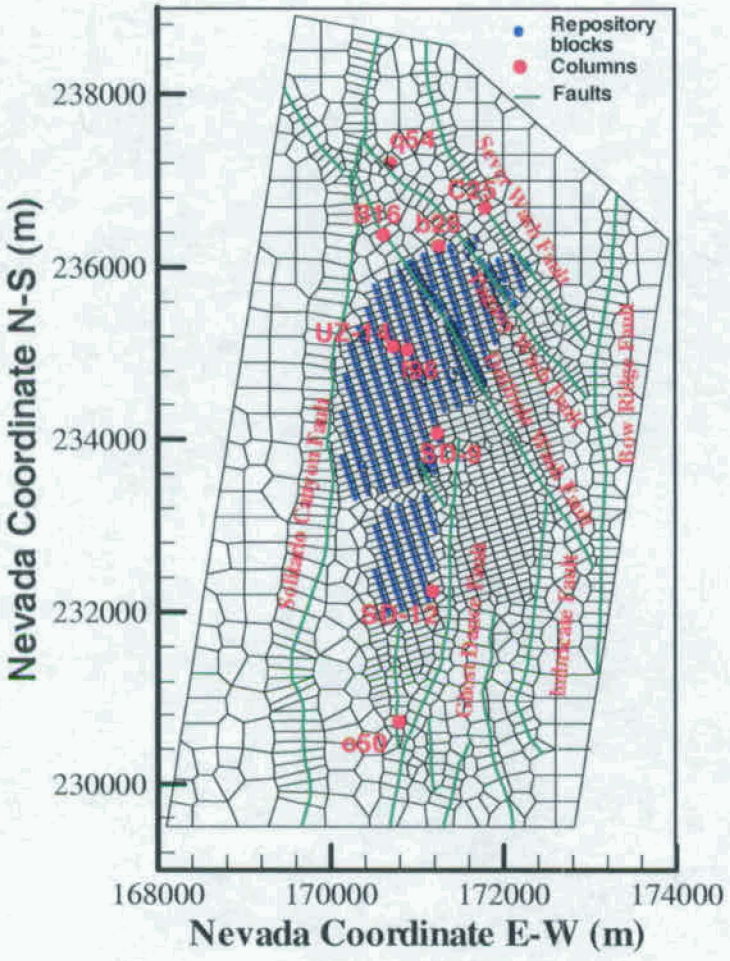

Figure 2. Plan view of the three-dimensional model grid, showing the model domain, faults incorporated, proposed repository footprint, and locations of columns to be investigated

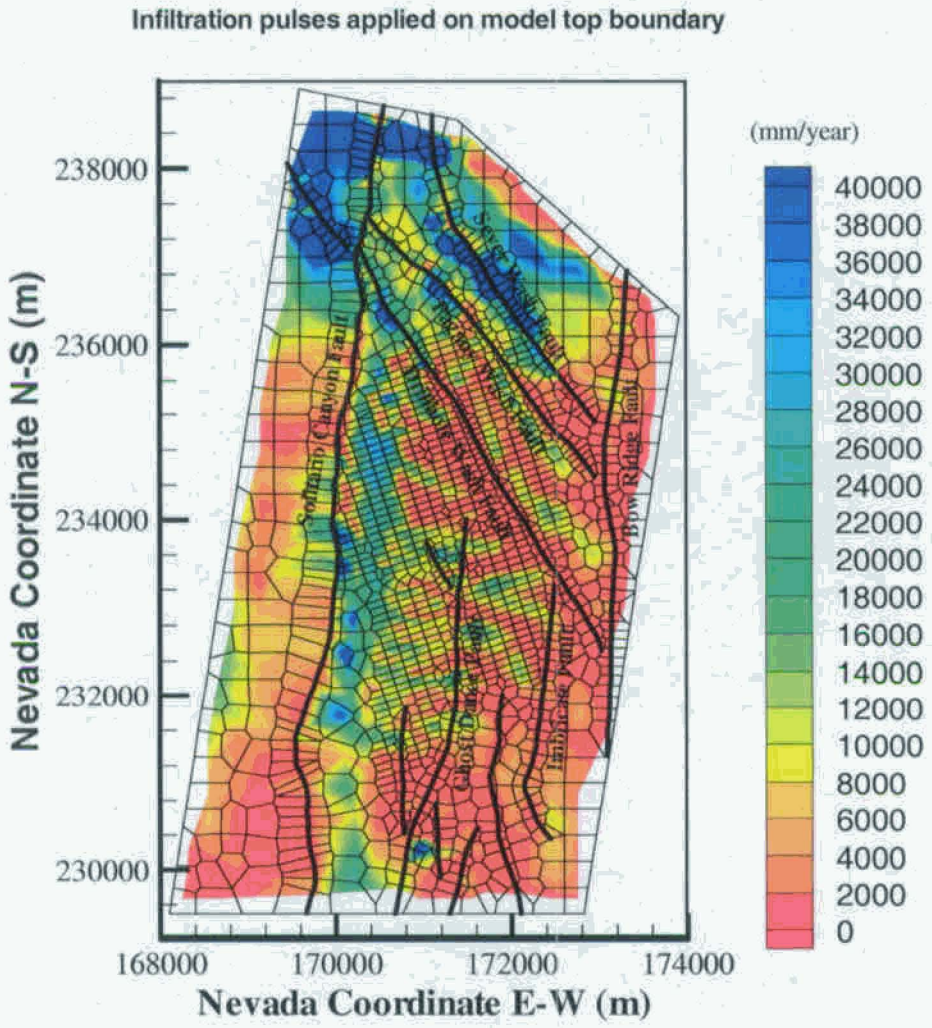

Figure 3. Spatial distribution of pulse infiltration applied over the 3-D model domain, equivalent to the case of present day mean infiltration

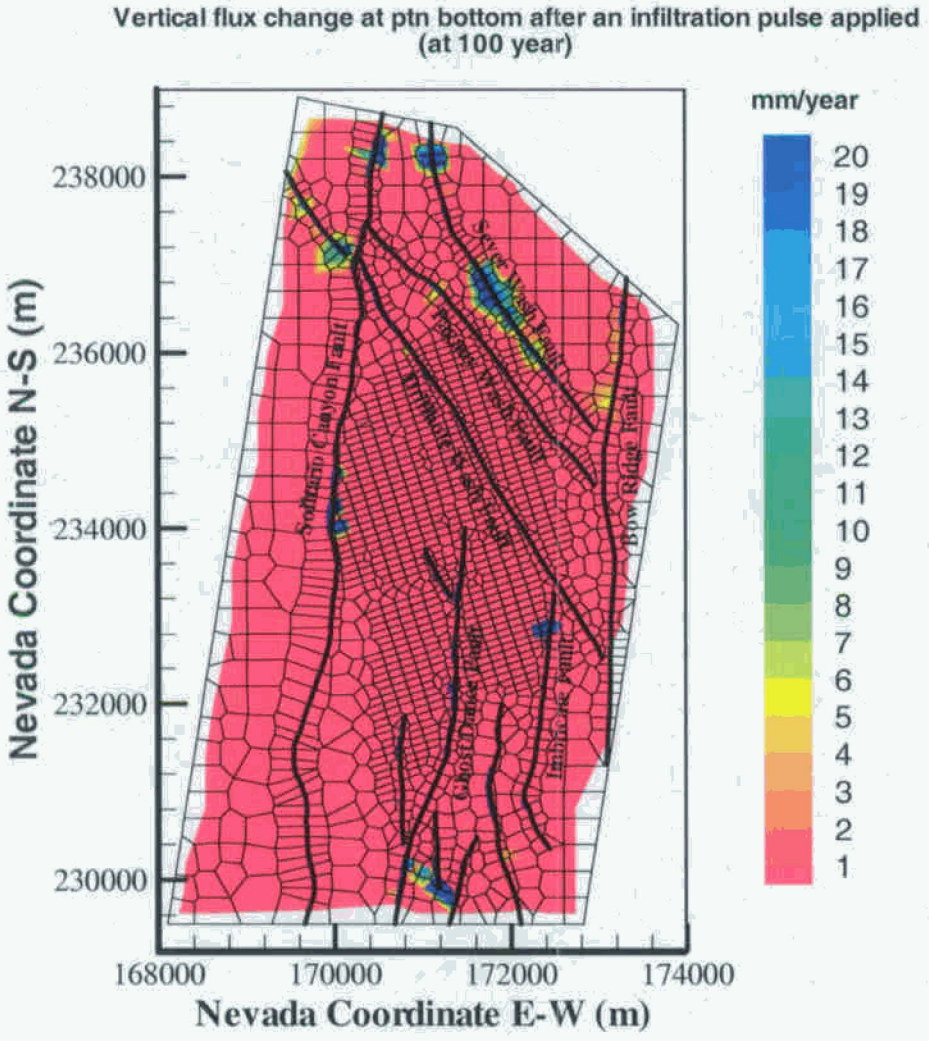

Figure 4 Change in percolation flux at the PTn bottom after 100 years when an infiltration pulse is applied on top boundary

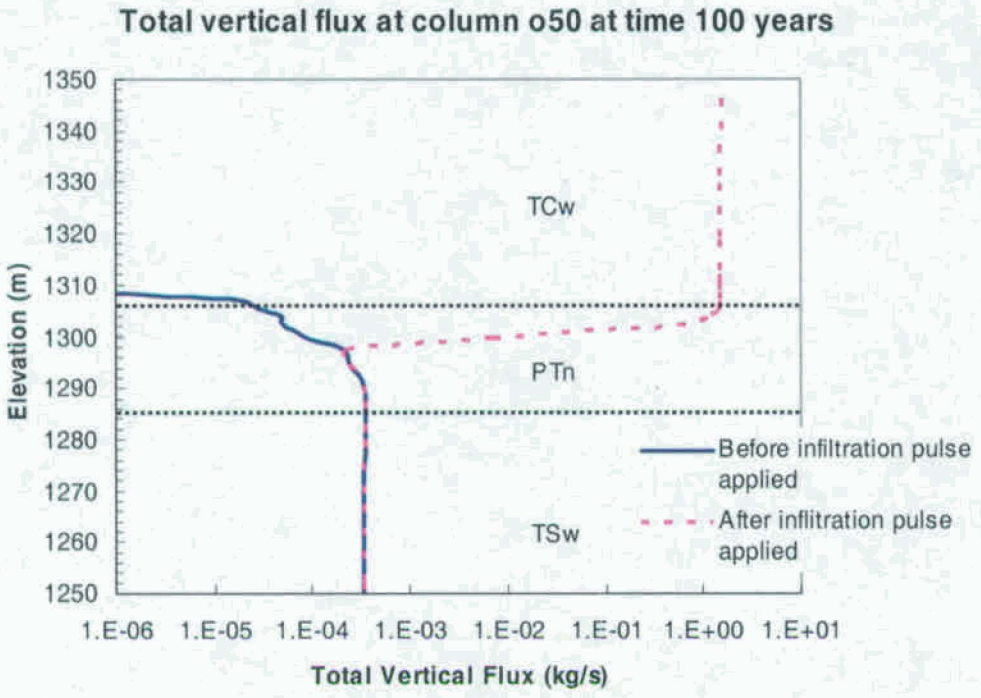

Figure 5. Percolation flux distribution along column o50, right before and after an infiltration pulse is applied at 100 years

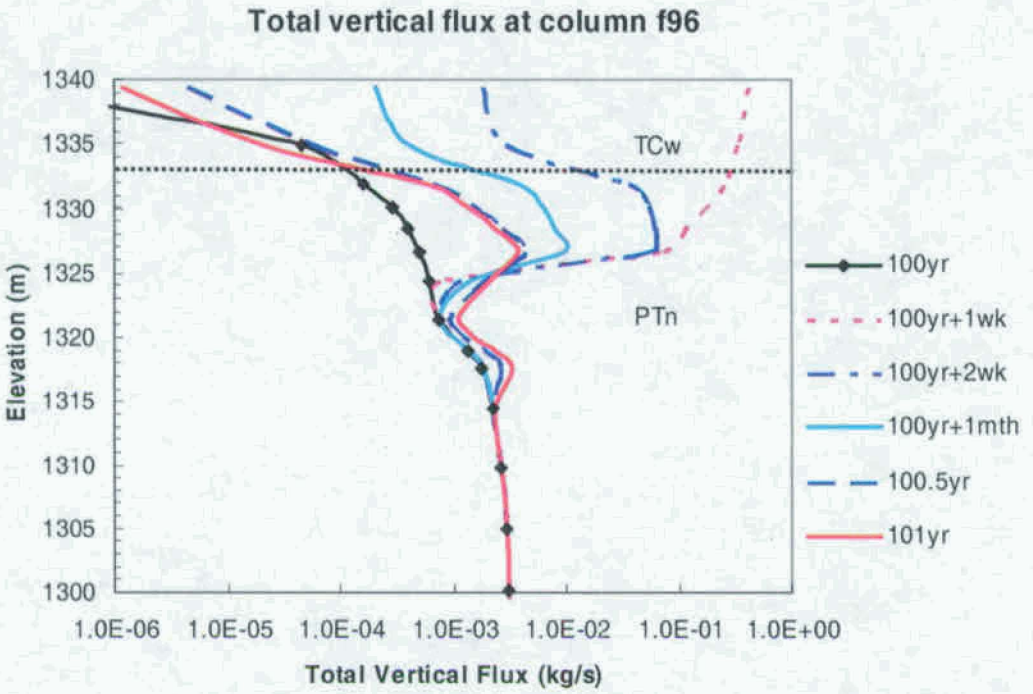

Figure 6. Flux distribution along column f96 at different times: right before infiltration pulse applied (100 years), and right after an infiltration pulse applied (100 years+1 week), and afterwards

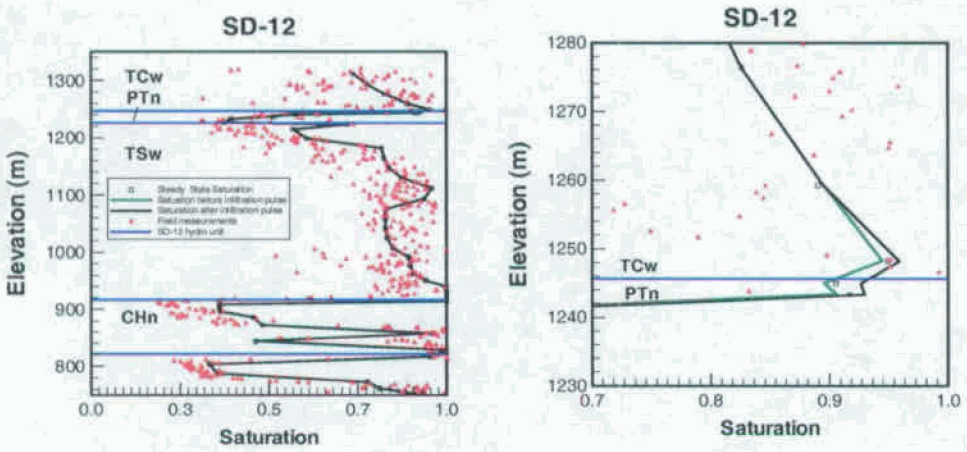

Figure 7. Matrix saturation distribution along column q47 (borehole SD-12) right before and after infiltration pulse applied at 100 years

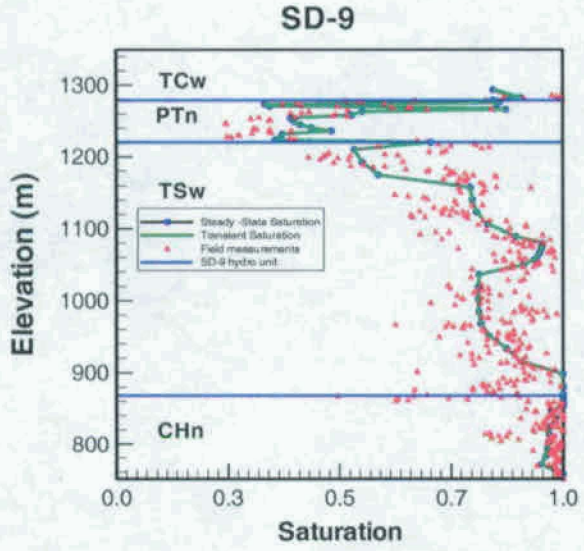

(a)

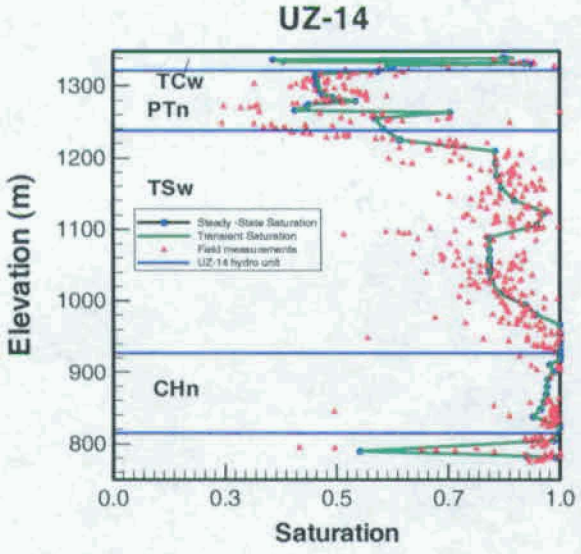

(b)

Figure 8. Comparison of simulated liquid saturations for episodic boundary condition and steady-state infiltration results with observed matrix liquid saturation for boreholes SD-9 and UZ-14

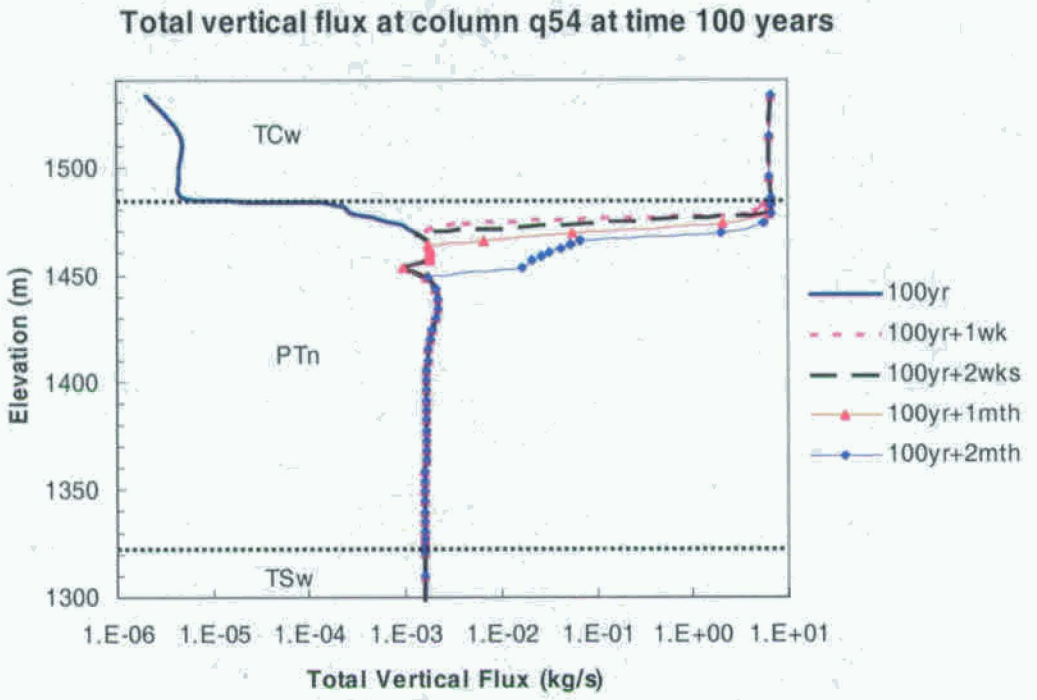

Figure 9. Flux distribution along column q54 for different lengths of infiltration pulses with the same average infiltration value at 100 years

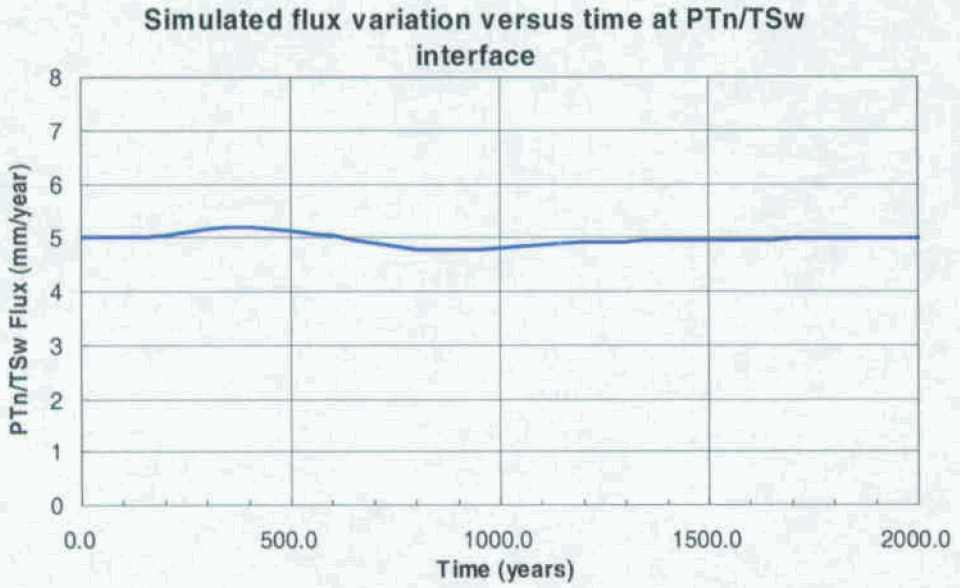

Figure 10. Simulated variations in total percolation fluxes versus times at the bottom of the PTn unit of the 1-D model, subject to one-week transient infiltration pulses every 50 years, equivalent to 5 mm/yr averaged infiltration rate

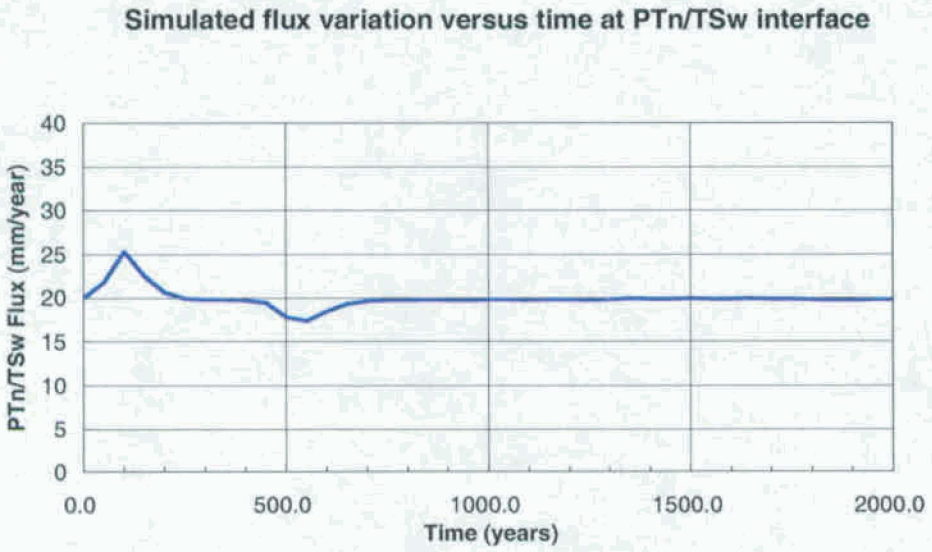

Figure 11. Simulated variations in total percolation fluxes versus times at the bottom of the PTn unit of the 1-D model, subject to one-week transient infiltration pulses every 50 years, equivalent to 20 mm/yr averaged infiltration rate

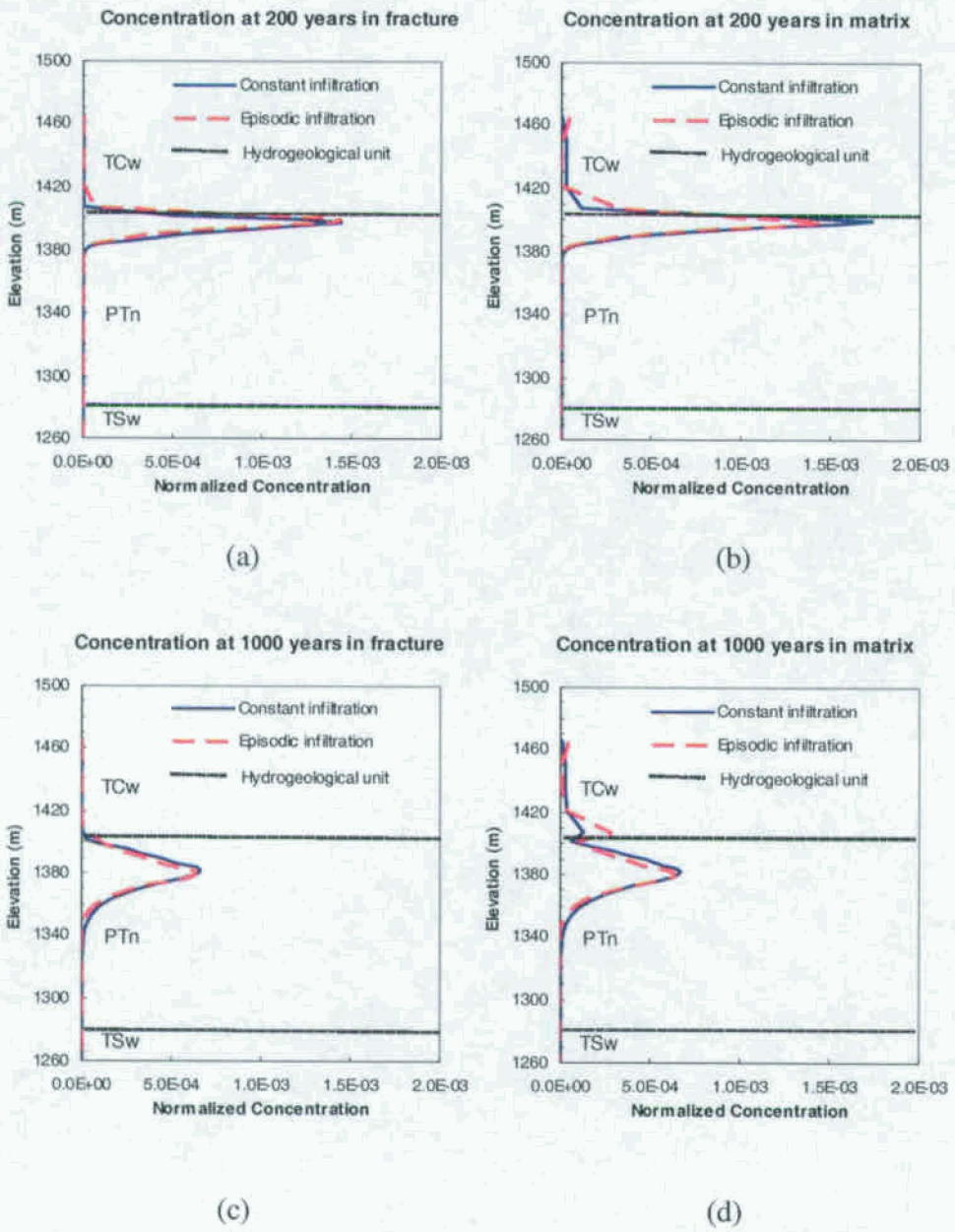

Figure 12. Simulated tracer concentration profiles; (a) in fracture, 200 years; (b) in matrix, 200 years; (c) in fracture, 1,000 years; and (d) in matrix, 1,000 years

Table 1. Relationship between major hydrogeologic units, geologic units, and model layers

Major Hydrogeologic Unit	Geologic Unit		UZ Model Layer
Tiva Canyon welded (TCw)	Tiva Canyon Tuff	Tpcr	tcw11
		Tpcp	tcw12
		Tpcpv3	tcw13
		Tpcpv2	
Paintbrush nonwelded (PTn)		Tpcpv1	ptn21
	Bedded tuff	Tpbt4	ptn22
	Yucca Mountain Tuff	Tpy	
			ptn23
			ptn24
	Bedded tuff	Tpbt3	
	Pah Canyon Tuff	Tpp	ptn25
	Bedded tuff	Tpbt2	ptn26
	Topopah Spring Tuff	Tptrv3	
		Tptrv2	

Table 2. Total simulated vertical percolation flux at the PTn bottom

Time (days)	Total Flux (kg/s)	
	Including flux in faults	Excluding flux in faults
7 (end of first infiltration pulse)	189.98	6.14
18262 (50 yrs, beginning of second infiltration pulse)	5.93	5.79
18269 (end of second infiltration pulse)	187.63	6.46
36524 (100 yrs, beginning of third infiltration pulse)	5.48	5.34
36531 (end of third infiltration pulse)	188.19	6.00

Table 3. Flux allocation in model columns at the beginning (100 years) and the end of the third pulse (100 years+1 week)

Column	Time	Flux in at top (kg/s)	Flux out at bottom (kg/s)	Lateral flow in/out (kg/s)	Water storage change (kg/s)
q47	100yr	0.00000E+00	-1.14450E-03	-1.04151E-04	-1.24865E-03
q47	100yr+1wk	1.32560E+00	-1.14450E-03	1.17974E+00	2.50419E+00
B16	100yr	0.00000E+00	-2.45245E-02	2.12014E-02	-3.32310E-03
B16	100yr+1wk	7.22390E+00	-2.45250E-02	-2.24046E-01	6.97533E+00
C25	100yr	0.00000E+00	-6.26497E-02	1.32931E-01	7.02812E-02
C25	100yr+1wek	1.51500E+01	-6.26480E-02	-4.63393E+00	1.04534E+01

Table 4. Flux changes in fracture and matrix at time of 1950 years, right after an infiltration pulse of 42.047 kg/s (52,180 mm/yr) applied on the 1-D model top boundary

Element	Model layer	Matrix storage change (kg)	Fracture storage change (kg)
M001Ab26	Tcw1	223,681.0	989,972.6
M0002b26	Tcw2	0.0	430775.1
M002Ab26	Tcw2	0.0	430768.8
M002Bb26	Tcw2	0.0	430630.2
M0003b26	Tcw3	2,928,519.6	447,046.8
M0004b26	Ptn1	2,610,507.1	165,593.0
M004Ab26	Ptn1	2,484,180.9	131,599.9
M004Bb26	Ptn1	2,326,273.1	106,405.1
M004Cb26	Ptn1	2,133,607.9	84,910.8
M0005b26	Ptn2	9,083,765.1	62,145.8
M005Ab26	Ptn2	223,249.3	6,395.2
M005Bb26	Ptn2	0.0	0.9
M0006b26	Ptn3	-109.8	-0.2
M006Ab26	Ptn3	-109.8	0.0
M006Bb26	Ptn3	-109.8	0.0
M006Cb26	Ptn3	-109.8	0.0
M006Db26	Ptn3	-109.8	0.0
total		22,013,234.8	3,286,244.0
Total mass change in fracture and matrix=25,299,478.8 kg Infiltration rate=42.047 kg/s Total infiltration in one week=25,430,026 kg			